Tellus (1988), *40A*, 257–271

Further modification of time-longitude lag-correlation diagrams: application to three-dimensional wave propagation

By WILLIAM J. RANDEL, *National Center for Atmospheric Research*, Boulder, CO 80307, USA*

(Manuscript received 24 August 1987; in final form 8 December 1987)

ABSTRACT

The time-longitude lag-correlation analysis of Fraedrich and Lutz is modified to include a second spatial dimension, thereby allowing coherent wave structure to be traced in time in the zonal-height or zonal-meridional planes. This technique is applied to daily hemispheric geopotential height data over 1000-1 mb for Northern and Southern Hemisphere winters. These analyses reveal vertical propagation of Rossby wavetrains from the troposphere into the stratosphere in midlatitudes; the correlation patterns suggest a downstream vertical splitting of the wave trains, with short horizontal scales confined to the troposphere. Zonal-meridional time-lag correlations of time-filtered data reveal the familiar teleconnection and stormtrack patterns seen in previous studies; similarities and differences between hemispheres are discussed.

1. Introduction

The observational analysis of coherently propagating fluctuations plays a central role in the understanding of atmospheric phenomena. The travelling and dispersive wavelike nature of midlatitude atmospheric fluctuations was noted shortly after hemispheric-scale upper air observations became available (Rossby, 1945), and Hovmöller (1949) developed the now famous time-longitude (or Hovmöller) diagram to quantify such observations. Fraedrich and Lutz (1987) (hereafter FL) have recently introduced a modified time-longitude diagram which uses statistical correlations to estimate zonal wavelengths, phase and group velocities (along constant latitude circles). The purpose of this paper is to propose a further modification to their method of analysis by including a second spatial dimension in the correlations (either height or latitude), thus allowing coherent fluctuations to be traced in the zonal-height or zonal-meridional planes. This modification is motivated by the observed three-dimensional nature of large-scale atmospheric wave propagation, i.e., 'great circle' horizontal energy propagation (discussed theoretically in Hoskins *et al.* (1977), and observationally in Blackmon *et al.*, 1984a, b) along with vertical wave energy propagation (Karoly and Hoskins, 1982; Randel, 1987).

The correlation analysis is developed and discussed in Section 2, followed in Section 3 application to both Northern and Southern Hemisphere winter geopotential height data. Vertical and meridional wave structure and propagation characteristics in both hemispheres are detailed; comparisons with previous analyses and between hemispheres are discussed.

2. Three-dimensional correlation analysis

Time lag correlation coefficients are calculated from anomalies (deviations from the time mean) of geopotential height $Z^*(\lambda,p,t)$, with respect to a chosen reference longitude (λ_0) and pressure (p_0), via

$$r(\lambda,p,\tau) = \frac{\frac{1}{N-\tau}\sum_{t=1}^{N-\tau} Z_0^*(\lambda_0,p_0,t)\cdot Z^*(\lambda,p,t+\tau)}{\sigma(Z_0^*)\cdot\sigma(Z^*)} \quad (1)$$

* The National Center for Atmospheric Research is sponsored by the National Science Foundation, USA.

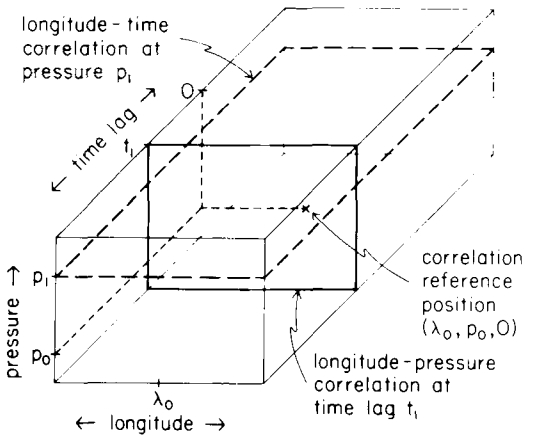

Fig. 1. Schematic diagram of three-dimensional correlation coefficients obtained from eq. (1). Two possible 2-dimensional slices through the correlation space are also illustrated by the heavy solid and heavy dashed lines.

Here N is the length of the available time series, τ is time lag, and σ denotes the square root of the variance of each time series. (Eq. (1) uses pressure as the third dimension, yielding information on the zonal-height time evolution; analogous calculations using lattitude reveal zonal-meridional statistics.)

The three-dimensional correlation coefficients obtained from eq. (1) are illustrated in Fig. 1. Although all the information could possibly be shown in a three-dimensional contour plot, a practical graphic method of display has not been found. Rather, groups of vertical slices through the correlation space at constant time lag allow depiction of coherent wave evolution in the longitude-pressure plane, while horizontal slices at constant pressure reveal longitude-time evolution, with respect to the reference pressure level p_0 (note that the horizontal slice at p_0 is identical to the longitude-time lag diagram of FL).

As discussed in FL and applied to the present situation, statistical estimates of horizontal or vertical wavelengths are given by twice the distance between maximum and minimum of the simultaneous coefficient (i.e., $\tau = 0$), while the movement in time of the maximum positive or negative correlation coefficients indicates a phase progression of the wave. Group velocity is recognized as a modulation of the strength of positive or negative correlations in time; this is clearly illustrated for a simple zonally propagating wave packet in FL. In a similar manner the present analyses allow phase and group velocities to be traced in the zonal-height (or zonal-latitude) plane. Additionally, the structure and time evolution of the longitude-height (or longitude-latitude) wave phase tilt is revealed by the present analyses.

3. Application to atmospheric data

3.1. Data and correlation significance levels

The data analyzed here are daily hemispheric geopotential height grids for 1000–1 mb. Grids from 1000–100 mb are NMC operational analyses, while geopotential heights from 70–1 mb are daily operational products from the Climate Analysis Center, Washington, DC. 90-day time series are obtained during Southern (July–September) and Northern (December–February) winters; 10° longitude grids are synthesized using zonal waves 0–12. Time filters applied here are the low-pass and band-pass filters designed for daily data introduced in Blackmon and Lau (1980); these filters retain fluctuations with time scales greater than 10 days and between 2–6 days, respectively. To allow for 21-point time filters to be applied, only the central 70 days of data are used in the correlation calculations. Correlation coefficients are averaged over eight winters (1979–1986) in each hemisphere. Because only 70-day time series are used each year, the seasonal cycle is not removed prior to the correlation calculations.

The correlations calculated from eq. (1) are referenced with respect to a particular longitude. Following FL, we calculate correlations at each of 36 longitudes around a constant latitude circle and average these together to produce correlation patterns independent of a particular longitude (computing cost can be saved by averaging over fewer equally-spaced reference longitudes — nearly identical results to those obtained here are found using 6 positions). Although such zonal averaging could confuse correlation patterns which are geographically fixed, this method is used here to study overall wave propagation characteristics, comparisons between hemispheres, and to simply illustrate the correlation technique.

Significance levels for the correlations presented here are estimated from a t-test, assuming $(8 \cdot 70/T_0)$ degrees of freedom (df) for each longitude reference position, where T_0 is a time scale between effectively independent observations. Furthermore, the simultaneous tropospheric correlation patterns suggest a zonal scale on the order of zonal wave 4 (or shorter for bandpass statistics), for which there is on the order of 20 df. This results in $(20 \cdot 8 \cdot 70/T_0)$ df for the zonally averaged correlations presented here. Using T_0 values of approximately (3, 2, 20) days for (unfiltered, bandpass, low-pass) statistics given in FL, this results in 99% significance levels near (0.042, 0.034, 0.109), respectively.

3.2. Longitudinal-vertical propagation

Fig. 2 shows a series of longitude-height sections at 51°N and 51°S of the correlation with respect to 300 mb, for time lags of −2, 0 +2 and +4 days (the correlation is 1.0 on the lag 0 plot at 300 mb and 0 degrees longitude). Correlations in Fig. 2 are calculated for unfiltered data. Overall the NH and SH patterns in Fig. 2 are similar, showing increased coherence with stratospheric levels at positive time lags and downstream (positive longitude differences) of the upper tropospheric reference position. The evolving patterns are indicative of vertically and eastward propagating wave trains, and this is consistent with the westward phase tilt exhibited by the strongest correlation patterns through the upper troposphore and stratosphere. There is also strong westward phase tilt with height in the lower troposphere (below 700 mb), strongest at time lags of −2 to 0 days.

The longitudinal scale of coherent fluctuations in the troposphere in Fig. 2 is on the order of 100° (near zonal wave 4), whereas the fluctuations in the stratosphere have a significantly longer scale (near 200°). The observed evolution is suggestion of selective transmission of planetary waves into the stratosphere, and trapping of shorter horizontal scales in the troposphere. Indeed, the SH patterns in Fig. 2 suggest a type of bifurcation, where part of the wave train propagates downstream into the stratosphere, and part is confined downstream in the troposphere. This vertical and downstream propagation and splitting of the wave train is in good agreement with the calculated response to isolated tropospheric forcing calculated by Held (1983); note especially the similarity of Fig. 2 with his Fig. 6.18. The SH patterns in Fig. 2 exhibit clear eastward phase progression at all levels, whereas the NH waves are quasi-stationary or slowly westward-moving in the stratosphere. Furthermore, the SH patterns exhibit stronger 'distant' correlations than those in the NH.

To highlight the time evolution, Fig. 3 shows longitude-time lag sections of the correlation with respect to 300 mb (the same reference point as in Fig. 2). The sections at 300 mb (Fig. 3 top) are time-longitude diagrams identical to those discussed in FL (their computations were for 500 mb and based on independent data), and nearly identical statistical estimates of zonal wavelengths, phase and group velocities are observed. Also shown in Fig. 3 are sections at 10 mb (with respect to the 300 mb reference position), highlighting the location of middle stratospheric fluctuations which are coherent with the 300 mb level. Negative (out-of-phase) correlation maxima are observed 60° downstream at time lags of 2–3 days in both the NH and SH. The NH exhibits in-phase correlation somewhat westward of the tropospheric reference position, this reflecting the westward tilt with height of the central correlation maximum (see Fig. 2). The SH patterns exhibit strong in-phase correlation approximately 150° downstream centered near a lag of +3 days; above 10 mb this region shows the strongest coherence with the troposphere (see Fig. 2 for lag of +4 days).

The vertical dispersion of different horizontal scales suggested in Fig. 2 prompts analysis of the vertical propagation characteristics of each zonal wavenumber separaely. Along these lines, one may construct groups of correlation diagrams similar to Figs. 2–3 for single zonal waves. A more concise method is afforded by the 'cross-spectral correlation analysis' of Randel (1987), which yields statistical estimates of coherence and phase in the meridional plane for individual zonal waves, and allows incorporation of time lag information. Fig. 4 shows height-time lag sections of the correlation coherence (equivalent to the correlation as in eq. 1) and phase (indicating longitude separation between wave crests at different pressure levels) with respect to 300 mb for zonal waves 1–3 separately, at 51°N and 51°S. Confidence intervals for these calculations are

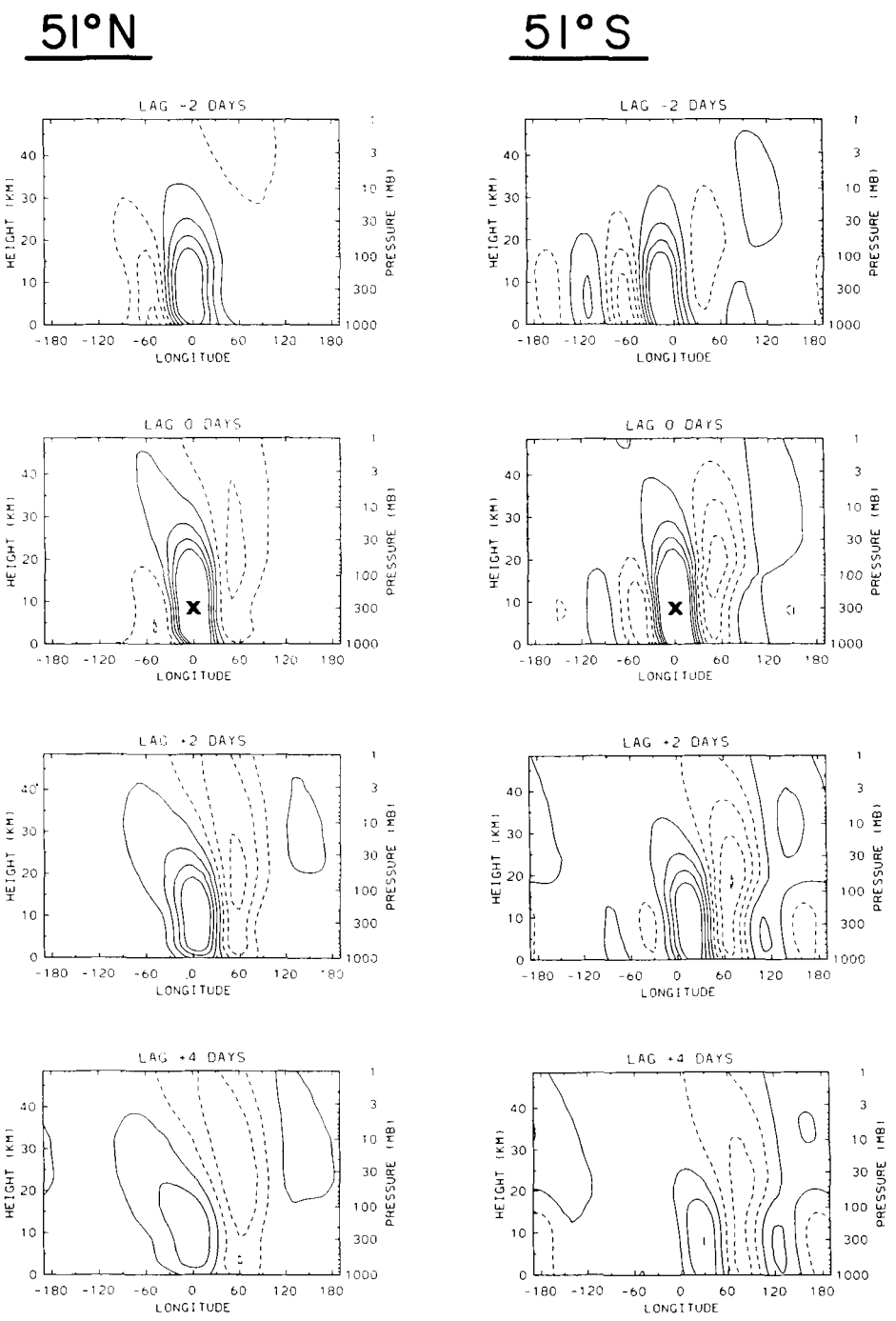

Fig. 2. Longitude-height sections at 51°N (left) and 51°S (right) of the correlation with respect to 300 mb, for time lags of −2, 0, +2, and 4 days (top to bottom). Because these are zonally-averaged statistics, the longitude scale refers to *relative* distance from the zero degree reference position (not geographic longitude). Contours are −0.45, −0.35, . . ., 0.35, 0.45. The reference position on this and the following figures is marked with an 'X' on the lag 0 plots.

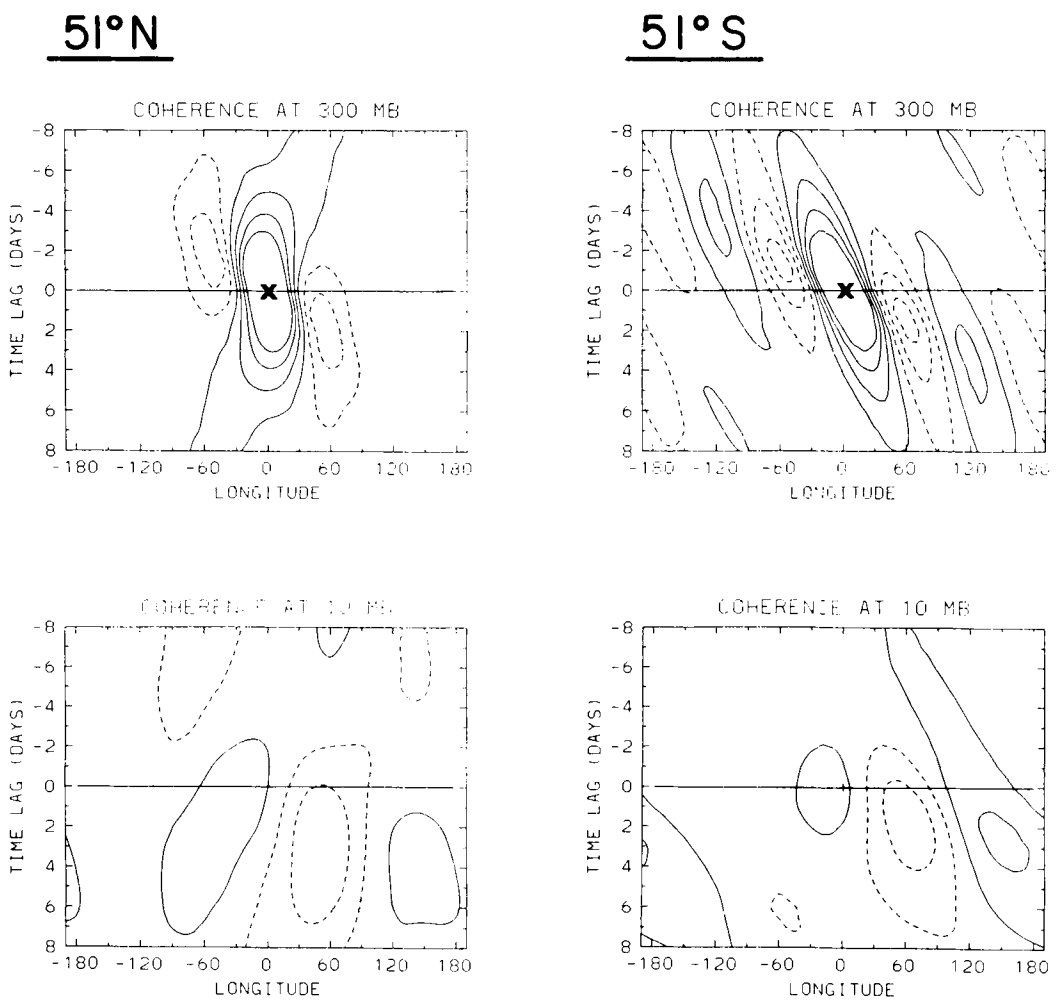

Fig. 3. Longitude-time lag sections at 300 mb (top) and 10 mb (bottom) of the correlation with respect to 300 mb, for 51°N (left) and 51°S (right). Contours as in Fig. 2. The 300 mb sections (top) are identical to the diagrams introduced in FL; the 10 mb sections reveal stratospheric fluctuations which are coherent with 300 mb.

discussed in Randel (1987); the 95% significance level for the correlations in Fig. 4 are near 0.2. These plots show significant coherence with the stratosphere at positive time lags, indicative of vertical propagation. Furthermore, there is a clear difference in the time scale of vertical propagation for each zonal wave: wave 1 shows strongest stratospheric coherence near a lag of 4 days, wave 2 near 2–3 days, and wave 3 near 0–2 days. These different time scales illustrate the dispersive behaviour of the waves. Additionally, the phase evolution in Fig. 4 shows the NH planetary waves to be westward propagating (wave 3 is quasi-stationary), whereas in the SH they are eastward moving (wave 1 is quasi-stationary).

Note the wave 1 signature in the SH in Fig. 4 shows a minimum in coherence between the tropospheric and stratospheric maxima coincident with a rapid vertical phase shift, signifying that the tropospheric and stratospheric wave 1 fluctuations are nearly out of phase. This behav-

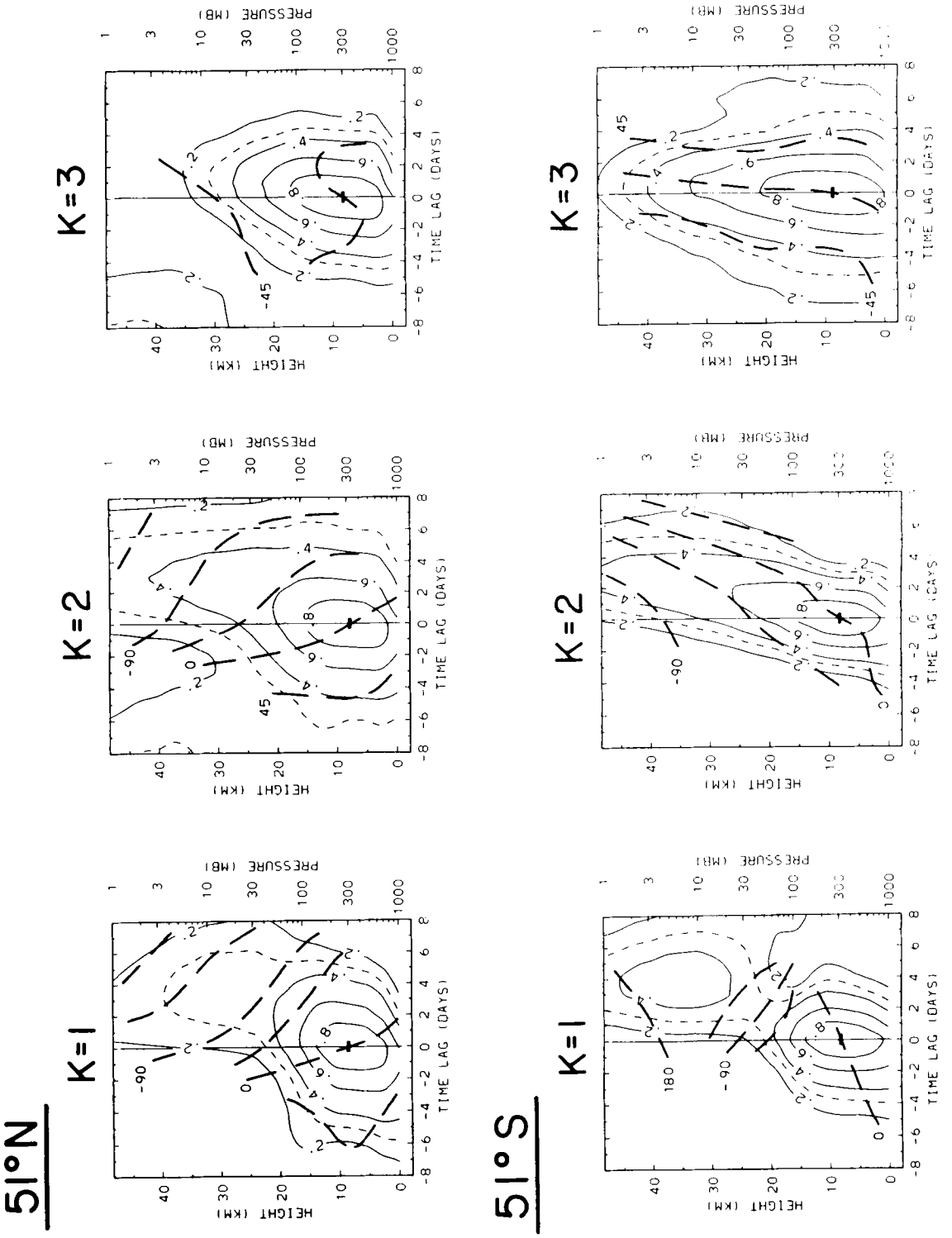
51°N
51°S
K=1
K=2
K=3
PRESSURE (MB)
HEIGHT (KM)
TIME LAG (DAYS)

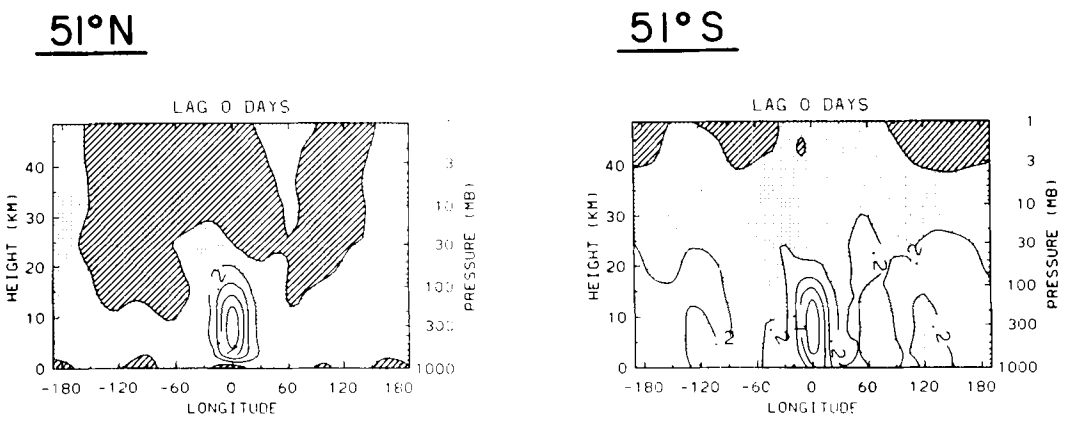

Fig. 5. Longitude-height cross sections of the standard deviation of correlation values, calculated from eq. (2), for a time lag of zero days for NH (left) and SH (right) data. These plots can be compared with the average lag 0 correlation patterns in Fig. 2. Contour interval of 0.05, with values above 0.2 stippled and values above 0.25 hatched.

iour is understood in light of Figs. 2 and 3, which shows the strongest positive correlation in the SH stratosphere to be nearly 180° downstream from the topospheric reference position. The wave 1 spectral signature of this is correlation maxima in the troposphere and stratosphere, with rapid vertical phase variation in between. Because the NH does not show such strong 'distant' correlation in the stratosphere, the spectral signature is one of slow westward phase tilt with height, and no minimum in the coherence is found (Fig. 4).

The correlation patterns in Figs. 2–3 are averages calculated from reference positions every 10° in longitude. The degree to which such patterns vary with longitudinal reference position may be assessed by computing the standard deviation of the separate correlation estimates via:

$$\sigma(\lambda,p,\tau) = \left[\frac{1}{(8\cdot 36-1)}\sum_{i=1}^{8}\sum_{l=1}^{36}(r_{i,l}(\lambda,p,\tau)-\bar{r}(\lambda,p,\tau))^2\right]^{1/2} \quad (2)$$

Here, $r_{i,l}(\lambda,p,\tau)$ denotes the correlation from eq. (1) for the ith year ($i = 1$–8 for the 8 years of data used here), and lth longitude reference position ($l = 1$–36 for reference longitudes every ten degrees), and $\bar{r}(\lambda,p,\tau)$ is the ensemble average correlation pattern (as in Fig. 2). In eq. (2), the effects of interannual variability are included with those due to different reference positions; the observed patterns mainly reflect the latter. Examples of such calculations are shown in Fig. 5 for the lag 0 plots in Fig. 2. The standard deviation is zero at the reference position (whereas each correlation is 1.0), increasing to values near 0.2–0.3 away from the central correlation maximum. The correlation standard deviations in Fig. 5 are relatively large compared with the average correlation values in Fig. 2, revealing a large amount of variability in the patterns with respect to different reference positions. Note, however, that the standard deviations in Fig. 5 are consistently smaller where the correlation maxima and minima in Fig. 2 are strongest; this shows less variability where the coherent fluctuations are most robust. Note also that the NH standard deviations in Fig. 5 are larger than those in the SH, a statistic which is consistent with the more pronounced zonal asymmetries in the NH. Similar standard deviation diagrams were computed for the other

Fig. 4. Height-time lag sections of the correlation, coherence and phase (discussed in text) for zonal wave 1 (left), 2 (middle), and 3 (right) fluctuations, with respect to the 300 mb level, at 51°N (top) and 51°S (bottom). Coherence contour interval of 0.2, with 0.3 contour added as a dashed line. Phase is indicated by heavy dashed lines, with a contour interval of 45°; a positive difference denotes eastward displacement.

correlations presented here, with results similar overall to those in Fig. 5; they are not discussed further.

Fig. 6 shows longitude-height sections as in Fig. 2, but for low-pass frequency (>10 days) fluctuations. Deep vertical penetration of the low-frequency waves are observed, with correlations similar overall to the unfiltered statistics. The similarity is not surprising in light of the large contribution of low-frequency motions to the total wave variance in the NH winter (Blackmon, 1976), although the results of Trenberth (1981) suggest there is more equal variance partitioning between high and low frequencies in the SH. The low-frequency patterns show eastward phase progression in the SH and quasi-stationarity in the NH. Note the rapid vertical phase variation in the lower troposphere for the NH patterns (particularly at lag −4 days), whereas the SH waves are more (but not completely) barotropic.

Fig. 7 shows similar cross sections for the bandpass (2–6 days) fluctuations. The NH and SH waves exhibit similar zonal scales and eastwood phase velocities in the troposphere, significantly different from the low frequency fluctuations. The patterns of correlation maxima and minima suggest upward and eastward propagation through the tropospheric wave train for both NH and SH. However, the patterns do not show deep downstream vertical penetration as that found for low-frequency waves (Fig. 6), although significant coherence up to 30 mb is seen in both hemispheres. The SH shows deeper vertical and farther downstream penetration than in the NH, and hints at a split wave train structure similar to that seen in Figs. 2 and 6.

3.3. Longitudinal-meridional propagation

Fig. 8 shows series of longitude-latitude sections (plotted on polar stereographic maps) of the 300 mb correlation with reference positions of 51°N and 51°S for unfiltered data. Note the correlation is 1.0 at longitude zero and 51°N on each of the lag 0 plots, and that the SH grids have been reversed so that eastward is still counterclockwise (for direct comparison with the NH statistics). These maps are similar to the one-point correlation maps of Wallace and Gutzler (1981), but are zonally-averaged quantities, not tied to any specific geographic location. The strongest correlations in the NH show patterns suggestive of great circle wave train routes. Blackmon *et al.* (1984a, b) have discussed the structure and evolution of such patterns extensively, using correlation maps at specific longitudes; they also presented zonal averaged statistics (their Figs. 11a,b) very similar to the patterns seen in Fig. 8. The evolving zonally-averaged patterns in Fig. 8 reveal two separate wave trains passing through middle latitudes that are usually not apparent at particular longitudes: both traverse from low to high to low latitudes, but pass the reference latitude (51°N) either before or after passing near the pole.

The SH patterns in Fig. 8 exhibit a strong zonally-oriented wave train, with a scale of zonal wave 4 and clear eastwood phase and group velocities. Furthermore, there are clear low-latitude (near 20°S) out-of-phase correlation maxima associated with the high-latitude wave train; overall the structure is distinctive to that seen in the NH. Fig. 9 shows similar diagrams, but for low-pass filtered statistics; both NH and SH patterns are very similar to those of the unfiltered data (Fig. 8).

Fig. 10 shows zonal-meridonal correlations calculated from bandpass-filtered data. Here the wave trains in both the NH and SH are clearly organized along latitude circles; such patterns are also extensively discussed in Blackmon *et al.* (1984a,b). As noted in regard to Fig. 7, the NH and SH bandpass fluctuations exhibit similar spatial and temporal scales, and the evolving signatures in Fig. 10 are quite alike (with somewhat stronger 'distant' correlations in the SH).

Fig. 10 shows clear downstream (eastward of the wave train center) meridional phase tilt of the waves, which acts to flux momentum poleward in both hemispheres; this is consistent with observations in the exit regions of localized NH storm tracks (Lau, 1978). Likewise, the strongest low-level westward phase tilts with height are observed in the center and somewhat upstream in Fig. 7, consistent with strong poleward heat flux in the middle and to the west of the storm track center (Lau, 1978). There is a clear indication in Fig. 10 of downstream equatorward propagation of the wave train at positive time lags; this behaviour is consistent with the aforementioned meridional wave phase tilts. Comparison with the low-pass correlations reveals meridional

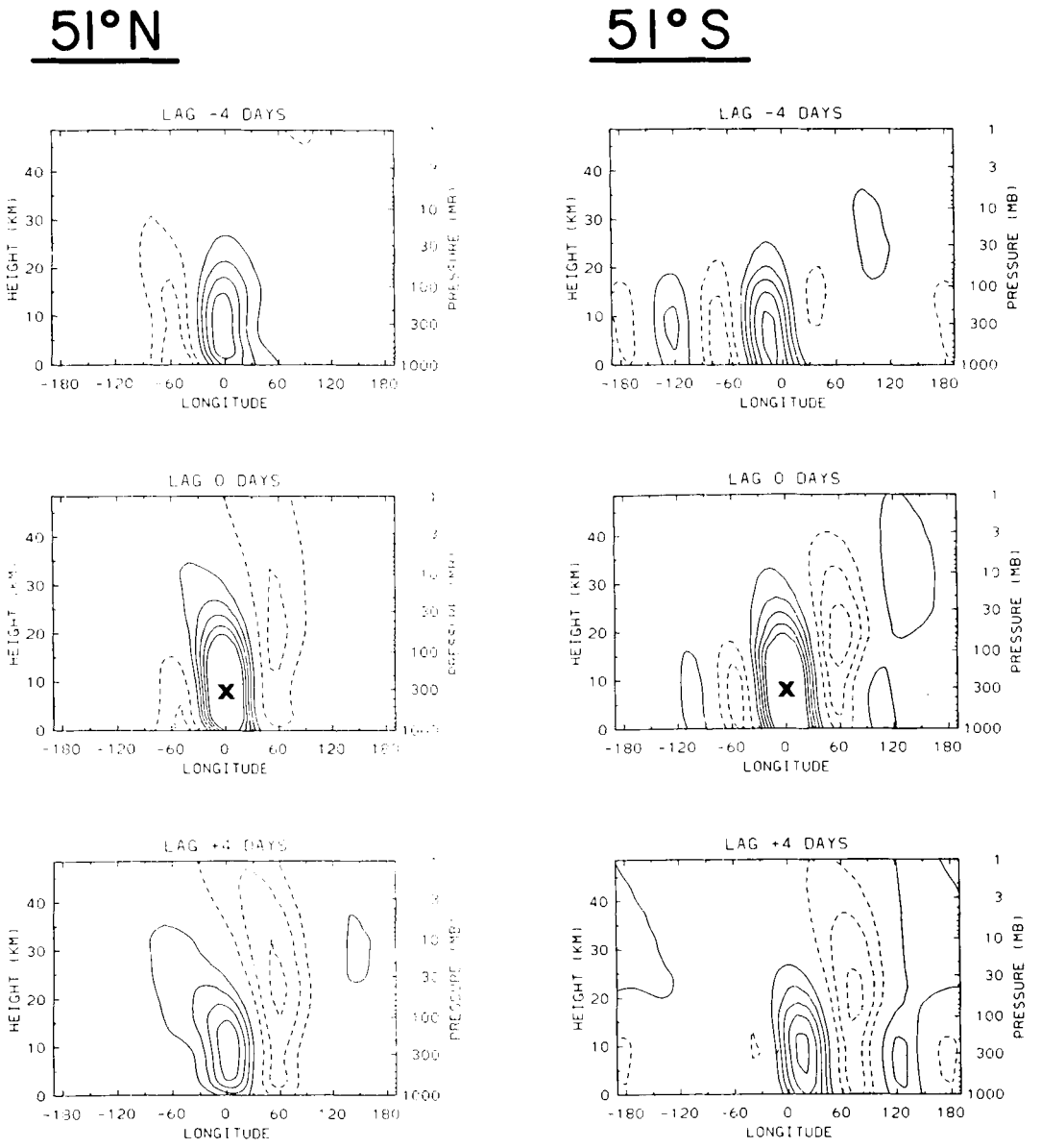

Fig. 6. As in Fig. 2, but for low-pass filtered data (periods greater than ten days). Contours of ± .1, .2, .3, .4, .5 (zero contours omitted).

elongation for the bandpass statistics versus more zonal elongation for low-frequency motions; the dynamical implications of such elongations (along with longitudinally local estimates) are given in Hoskins et al. (1983).

Fig. 11 shows a series of sections tracing horizontal wave propagation in the middle stratosphere (10 mb) of both winter hemispheres. Coherent fluctuations in the stratosphere are on the planetary scale, with out-of-phase, predominantly

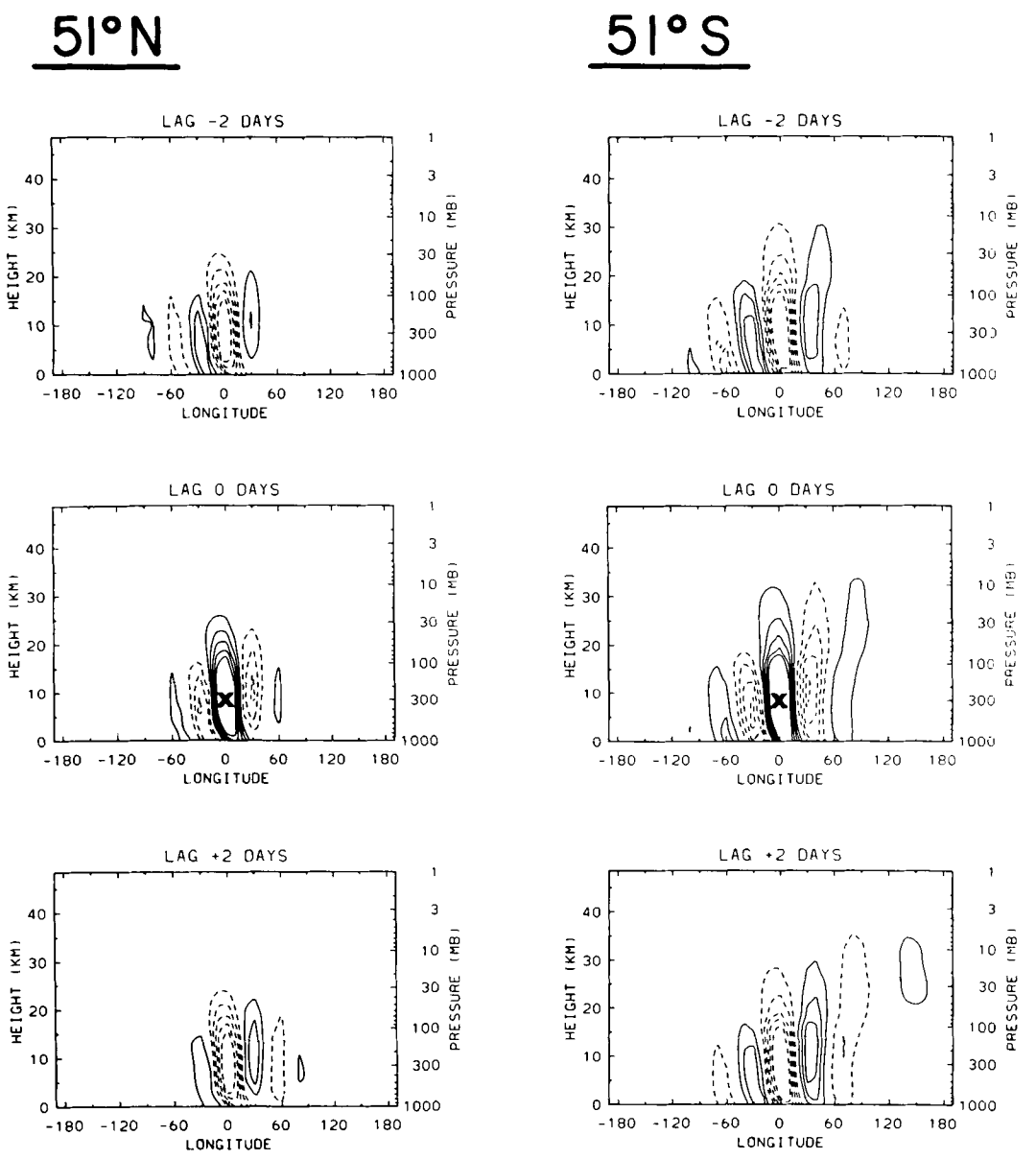

Fig. 7. As in Fig. 6, but for bandpass filtered data (periods of 2–6 days).

zonally-symmetric fluctuations in low latitudes of both hemispheres (much stronger in the NH). There is a clear eastward propagating zonal wave 2 pattern in the SH, while the NH exhibits more complex horizontal structure with quasi-stationary behaviour. The modulated correlation patterns reveal evidence of eastward group velocity in both hemispheres.

4. Summary

The examples here are intended to illustrate the utility of the present analysis technique to the study of 3-dimensional wave propagation. Such statistics can be calculated with respect to a particular longitude to study geographically-fixed phenomena, or they can be calculated and

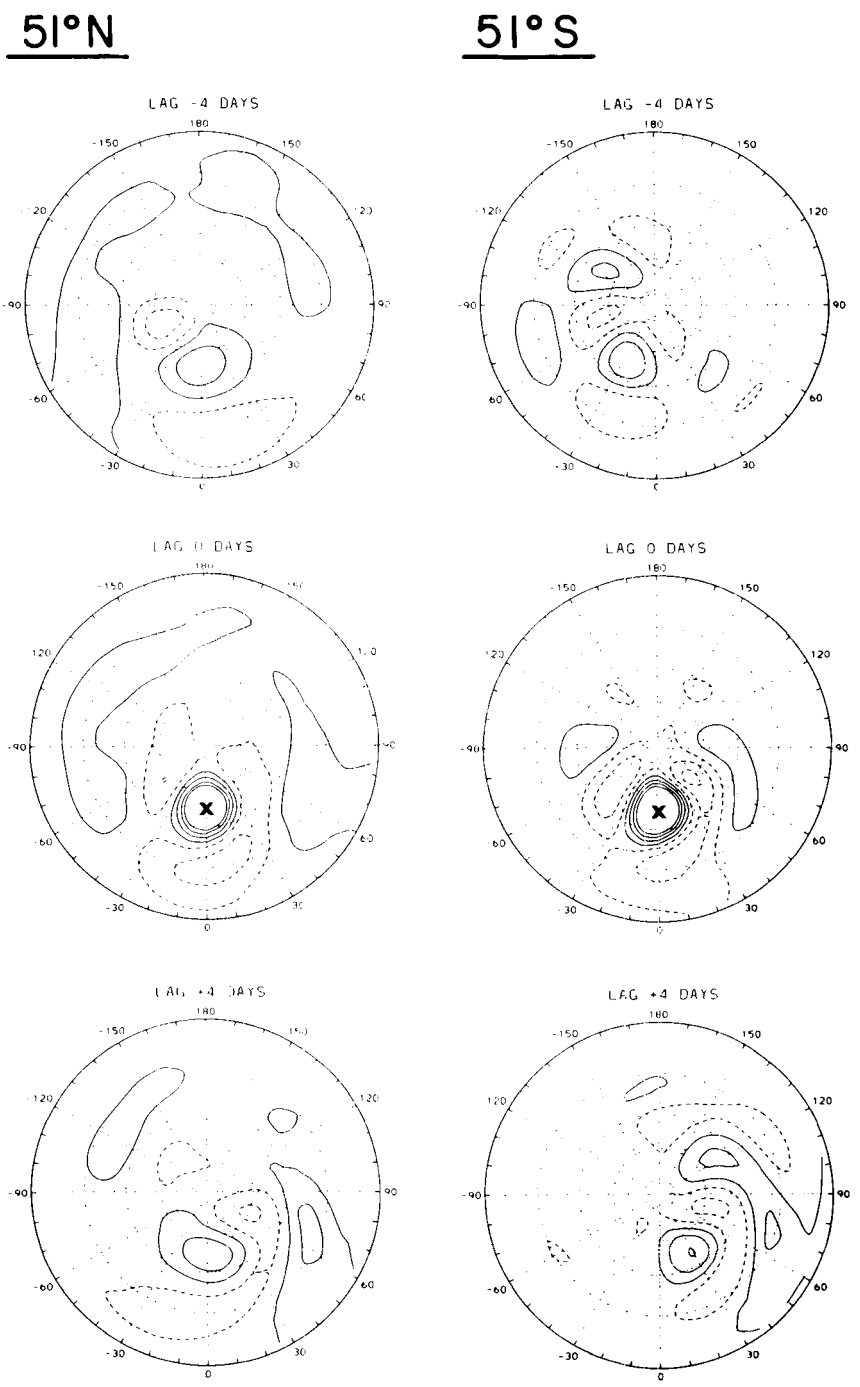

Fig. 8. Longitude-latitude sections at 300 mb of the correlation with respect to 51°N (left) and 51°S (right) plotted on polar stereographic grids (latitudes are drawn every 20 degrees — the outermost latitude is the equator). As in Fig. 2, the longitude scale denotes relative distance from the zero degree (6 o'clock) reference position, eastward is counterclockwise. The SH polar grids have been reversed (so that eastward is counterclockwise) to facilitate comparison with the NH diagrams. Contours as in Fig. 2.

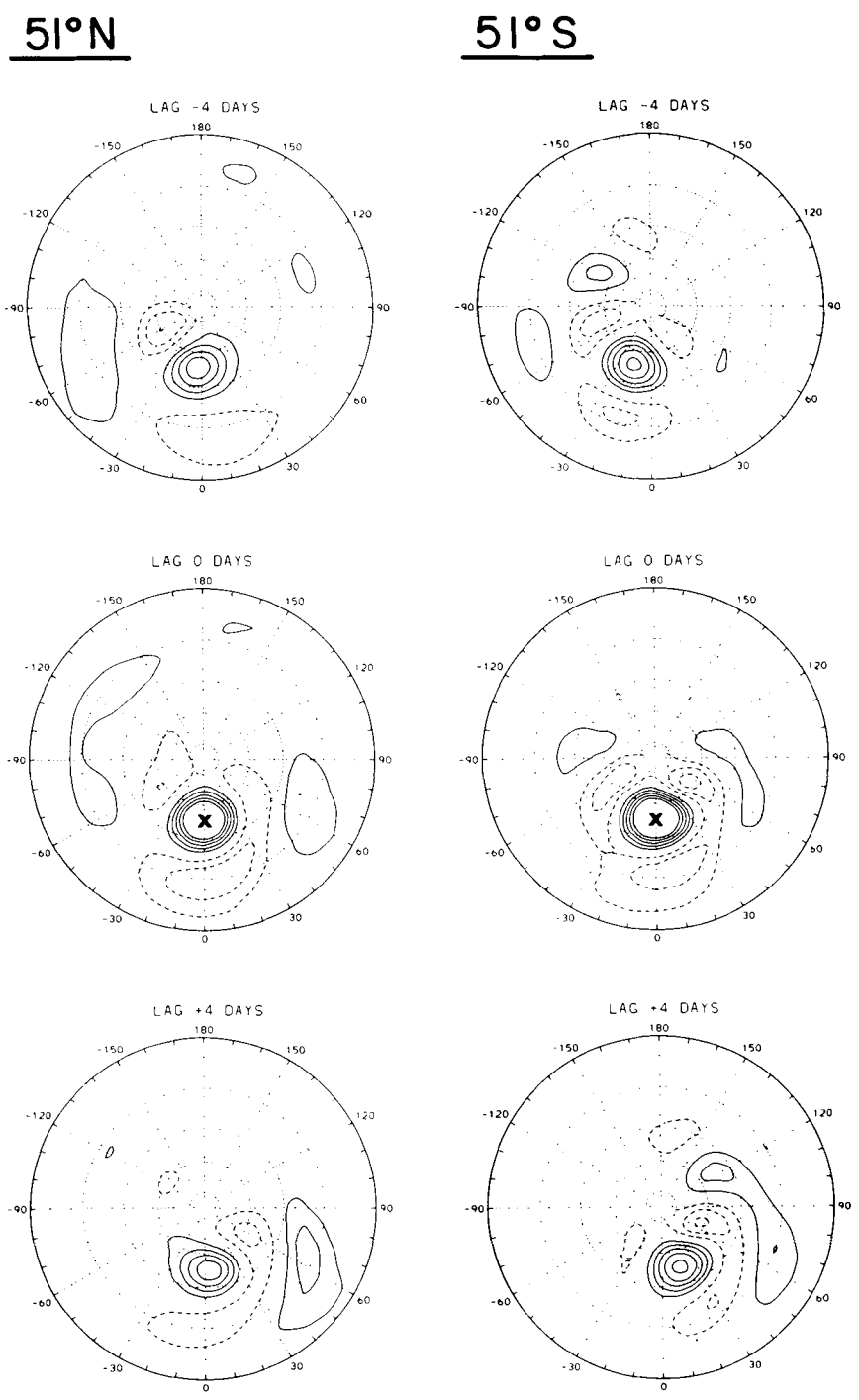

Fig. 9. As in Fig. 8, but for low-pass filtered data (periods greater than ten days). Contours as in Fig. 6.

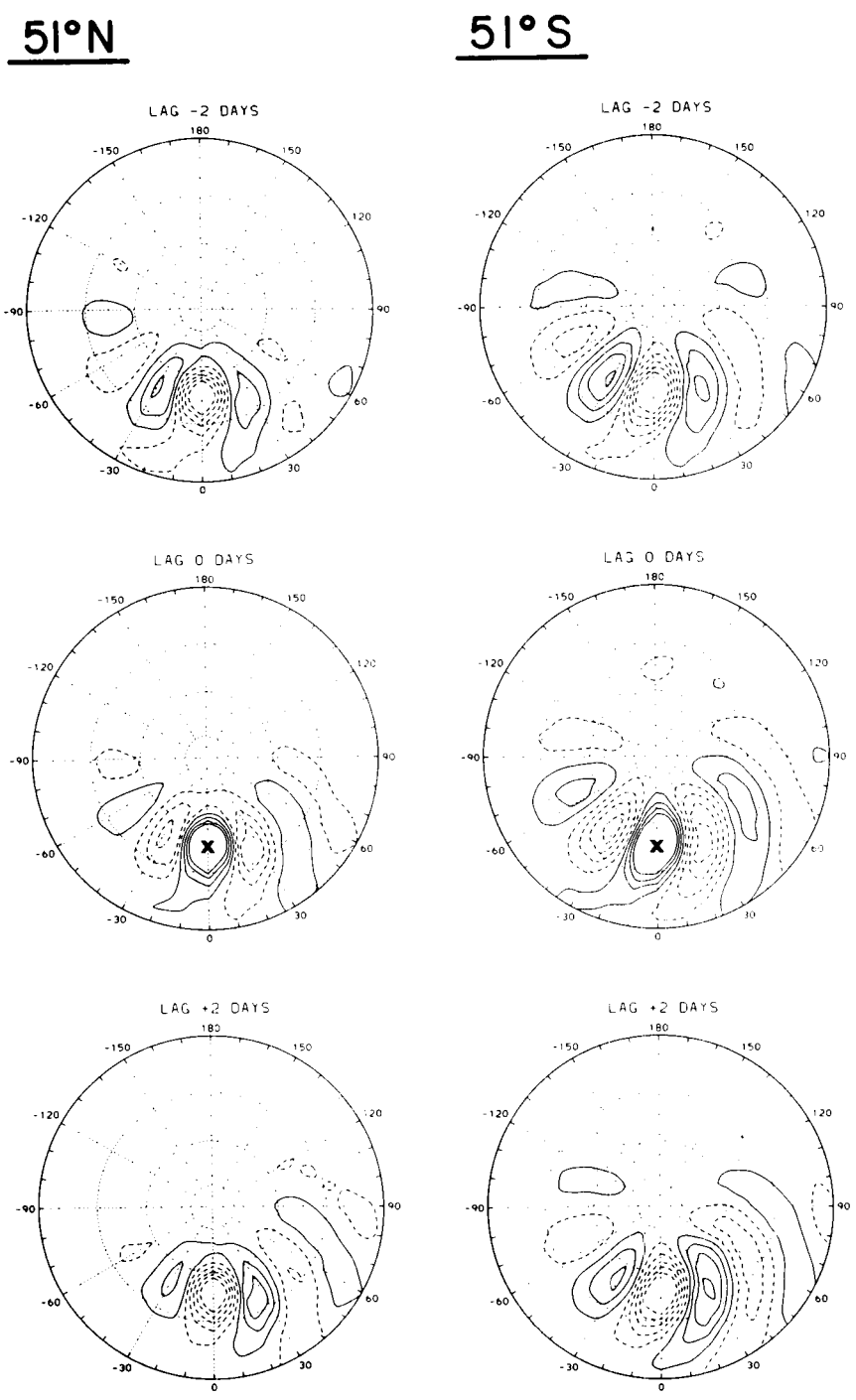

Fig. 10. As in Fig. 8, but for bandpass-filtered data (periods of 2-6 days). The outermost latitude on these diagrams is 20°N (left) and 20°S (right).

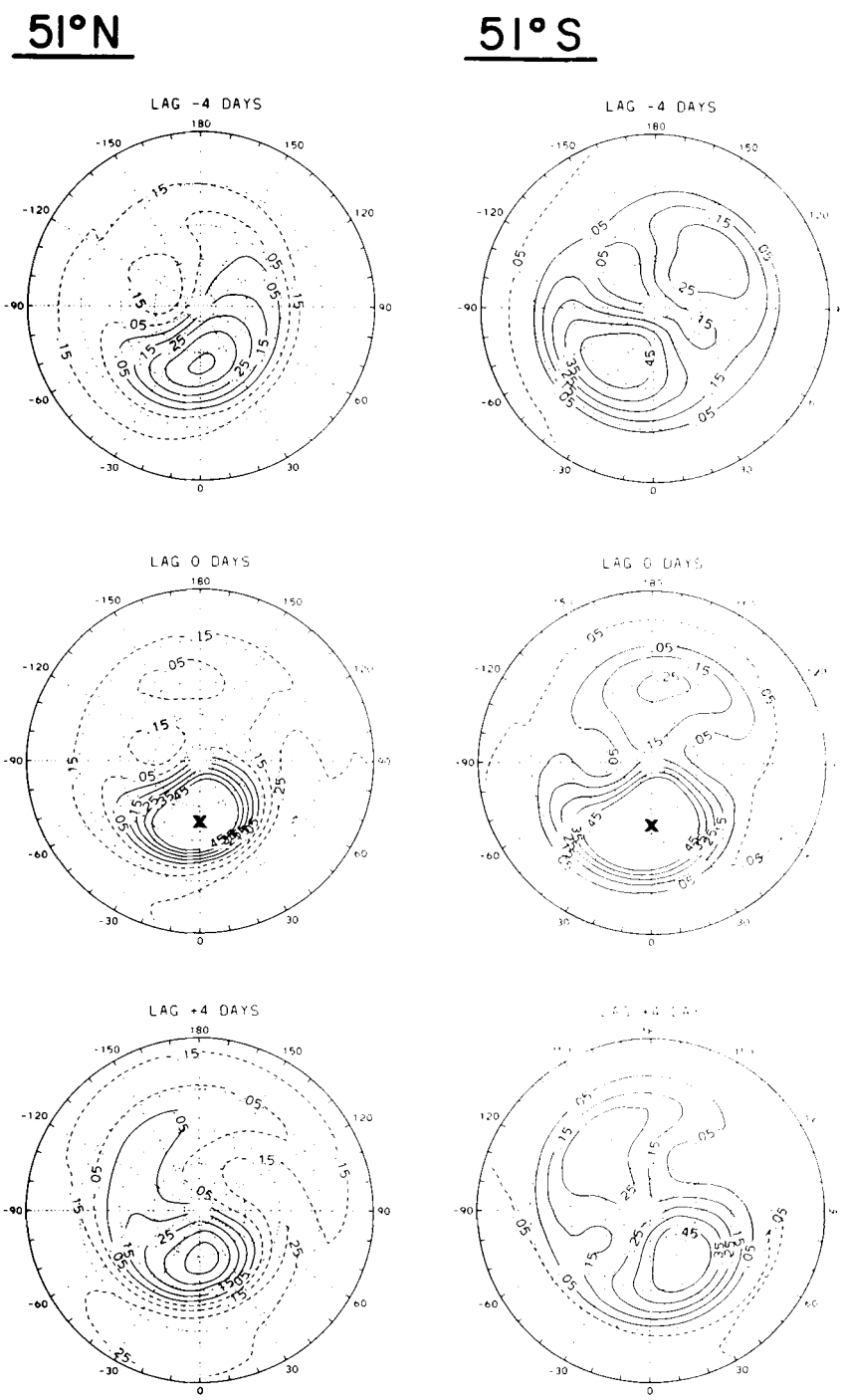

Fig. 11. As in Fig. 8, but for 10 mb correlations (using unfiltered data) at 51°N (left) and 51°S (right).

averaged with respect to several longitudes (as were the zonally-averaged calculations presented here). Groups of horizontal or vertical slices through the three-dimensional correlation space yield statistical estimates of instantaneous structure and evolution of coherent fluctuations in the data.

Although the horizontal dispersion of wave energy has been stressed in many previous studies (e.g., Hoskins *et al.*, 1977; Wallace and Gutzler, 1981; Blackmon *et al.*, 1984a,b), the correlation statistics shown here reveal just as strong "distant" correlations for vertical wave propagation between the troposphere and middle stratosphere (in midlatitudes during winter). This shows that vertical propagation is a fundamental aspect of midlatitude disturbances during winter, and is a feature that should be simulated correctly in forecasts or numerical models. The correlation analyses discussed here provide one method of analyzing and verifying such behaviour.

5. Acknowledgements

The author thanks Drs. Maurice Blackmon and Steven Mullen for helpful comments on an earlier version of this work.

REFERENCES

Blackmon, M. L. 1976. A climatological spectral study of the 500 mb geopotential height of the Northern Hemisphere. *J. Atmos. Sci. 33*, 1607–1623.

Blackmon, M. L. and Lau, N. C. 1980. Regional characteristics of the Northern Hemisphere wintertime circulation: A comparison of the simulation of a GFDL general circulation model with observations. *J. Atmos. Sci. 37*, 497–514.

Blackmon, M. L., Lee, Y.-H., Wallace, J. M., and Hsu, H.-H. 1984a. Time variation of 500 mb height fluctuations with long, intermediate, and short time scales as deduced from lag-correlation statistics. *J. Atmos. Sci. 41*, 981–991.

Blackmon, M. L., Lee, Y.-H. and Wallace, J. M. 1984b. Horizontal structure of 500 mb height fluctuations with long, intermediate, and short time scales. *J. Atmos. Sci. 41*, 961–979.

Fraedrich, K. and Lutz, M. 1987. A modified time-longitude diagram applied to 500 mb heights along 50° north and south. *Tellus 39A*, 25–32.

Held, I. M. 1983. Stationary and quasi-stationary eddies in the extratropical troposphere: Theory. In *Large-scale dynamical processes in the atmosphere* (ed. B. J. Hoskins and R. P. Pearce). Academic Press, 397 pp.

Hoskins, B. J., Simmons, A. J. and Andrews, D. G. 1977. Energy dispersion in a barotropic atmosphere. *Quart. J. Roy. Meteor. Soc. 103*, 553–567.

Hoskins, B. J., James, I. and White, G. H. 1983. The shape, propagation and mean flow interaction of large-scale weather systems. *J. Atmos. Sci. 40*, 1595–1612.

Hovmöller, E. 1949. The trough-and-ridge diagram. *Tellus 1(2)*, 92–66.

Karoly, D. J. and Hoskins, B. J. 1982. Three-dimensional propagation of planetary waves. *J. Meteor. Soc. Japan 60*, 109–122.

Lau, N. C. 1978. On the three-dimensional structure of the observed transient eddy statistics of the Northern Hemisphere wintertime circulation. *J. Atmos. Sci. 35*, 1900–1923.

Randel, W. J. 1987. A study of planetary waves in the Southern winter troposphere and stratosphere. Part I: Wave structure and vertical propagation. *J. Atmos. Sci. 44*, 917–935.

Rossby, C.-G. 1945. On the propagation of frequencies and energy in certain types of oceanic and atmospheric waves. *J. Marine Res. 2*, 187–204.

Trenberth, K. E. 1981. Observed Southern Hemisphere eddy statistics at 500 mb: Frequency and spatial dependence. *J. Atmos. Sci. 38*, 2585–2605.

Wallace, J. M. and Gutzler, D. S. 1981. Teleconnections in the geopotential height field during the Northern Hemisphere winter. *Mon. Wea. Rev. 109*, 785–812.